THE AFFINE PROJECTION MODEL FOR SENSOR ORIENTATION: EXPERIENCES WITH HIGH-RESOLUTION SATELLITE IMAGERY

T. Yamakawa , C.S. Fraser

Department of Geomatics, University of Melbourne, Melbourne VIC 3010, Australia
yamakawa@sunrise.sli.unimelb.edu.au, c.fraser@unimelb.edu.au

Commission I, WG V/5

KEY WORDS: Sensor orientation, high resolution satellite imagery, affine projection, IKONOS, QuickBird

ABSTRACT:

Accompanying the successful deployments of the IKONOS and QuickBird high-resolution satellite imagery (HRSI) systems have been a number of investigations into the utilisation of HRSI for the extraction of precise 3D metric information. Among the promising 'alternative' sensor orientation models investigated has been an approach based on affine projection. This model has previously been reported as performing well in experiments with stereo configurations of IKONOS imagery. In situations where precise sensor and orbital information is not fully accessible, empirical sensor orientation models requiring only a modest number of ground control points become an attractive proposition. This paper briefly summarises the theory and validity of the affine model as configured for application to sensor orientation and geopositioning for HRSI. The results of experiments with three HRSI stereo scenes are also presented, in which sub-pixel accuracy was achieved from both IKONOS and QuickBird imagery.

1. INTRODUCTION

The determination of sensor orientation models to support photogrammetric exploitation of satellite imagery has been an active research topic for around two decades. As the most rigorous approach, collinearity-based mathematical models have in the past been proposed and successfully applied for medium-resolution imaging systems such as SPOT, MOMS and IRS. These models describe the rigorous geometry of the scanner, utilising knowledge of the satellite trajectory and sensor calibration data. Therefore, access to the camera model and orbit ephemeris data is indispensable for their successful application. In circumstances where the policy of the HRSI vendor does not permit access to the camera model and orbital data, the collinearity-based approach is generally not a viable proposition.

As a substitute for rigorous sensor models, a number of 'alternative' or 'replacement' models have been proposed. The best known and currently most widely utilised of these is the rational function model (also termed rational polynomial camera model or rational polynomial coefficients, and abbreviated to RFM, RPC or RPCs). A set of polynomial coefficients provided by the satellite imagery vendor is accurately computed from the rigorous sensor model. RPCs have gained popularity as a replacement for the rigorous sensor model for HRSI (Fraser & Hanley, 2004; Grodecki & Dial, 2003). A further alternative sensor orientation model is based on affine projection. This was initially applied with success to the orientation of SPOT and MOMS-2P imagery (Hattori et al., 2000; Okamoto et al., 1998; 1999), and it has characteristics that indicate suitability for HRSI.

The authors have been involved in a number of investigations centred upon assessment of the affine sensor orientation model for HRSI (Hanley et al., 2002; Fraser et al., 2002; Fraser & Yamakawa, 2004). The overall results have indicated that the affine model achieves sub-pixel to 1-pixel level accuracy for Reverse-scanned IKONOS stereo configurations and even for IKONOS multi-strip configurations. In spite of these encouraging results, there have always been several concerns about the applicability of the model. These especially focus upon its lack of rigour and its likely shortcomings when the satellite imaging system does not perform in a linear manner. Justifiable questions therefore remain about how universally applicable the affine model is for HRSI sensor orientation.

In this paper we summarize recent experiences with the affine model for sensor orientation and geopositioning from IKONOS and QuickBird imagery. The paper is divided into two parts. The first part covers important issues involved in sensor orientation modelling based on affine projection. The second presents results of experimental application with one IKONOS *Geo* and two QuickBird *Basic* stereo image pairs. These will highlight both advantages and shortcomings of the affine model approach.

2. THEORY OF AFFINE PROJECTION

The standard formulation of the affine model is expressed as a linear transformation from 3D object space (X, Y, Z) to 2D image space (x, y):

$$\begin{aligned} x &= A_1 X + A_2 Y + A_3 Z + A_4 \\ y &= A_5 X + A_6 Y + A_7 Z + A_8 \end{aligned} \qquad (1)$$

where $A_1 – A_8$ = parameters describing rotation (3), translation (2) and non-uniform scaling and skew distortion (3)
x, y = coordinates in line and sample direction
X, Y, Z = object coordinates

Equation 1 can be interpreted in several ways. It can be viewed, for instance, as a 3D affine transformation followed by an orthogonal projection, as a 3D similarity transformation followed by a skew parallel projection, or as a skew parallel projection followed by a similarity transformation. In the application of the affine projection model, it is useful to consider its connection to the central-perspective model, i.e. a departure from collinearity equation. In fact, the introduction of the common scale factor is the key to converting the non-linear collinearity equation to a form of simple linear transformation. The affine model is a further generalised form, which allows affinity (non-uniform scaling and skew distortion) in the image to object space transformation.

In 3D scene reconstruction, a model formed by a stereo pair of affine images can be created from four corresponding (conjugate) points, and can be related to the object space by a 3D affine transformation (twelve degrees of freedom). On the other hand, for the special case of central perspective projection where the internal geometry is known, five points are required to form a model which is then transformed to object space by a similarity transformation (seven degrees of freedom). The distinction between these two approaches lies in the inclusion or omission of affinity and different scale factors in each axis of the model space. To form a model of correct shape from affine images, constraints describing orthogonality and uniform scaling have to be imposed among the affine parameters. Also, a third image has to be added to the network to resolve ambiguity arising from the adoption of a common scale factor (Ono & Hattori, 2003).

For satellite line scanner imagery, however, these constraints can be neglected because of the geometry of pushbroom scanners. With narrow field of view imaging systems, uncertainties and perturbations of the sensor and other parameters of affine distortion rarely assume significance. This also allows constraint-free application of the affine model to processed imagery (eg rectified) as well as raw scanner imagery.

3. MODEL VALIDITY

In the previous section, the affine model was presented as a 2D camera model. However, the geometry of a line scanner is based on a central-perspective projection. More precisely, it is comprised of a one-dimensional central-perspective projection in the scanning direction and an approximately parallel projection in the satellite track direction. Therefore, in the application of the affine model to line scanner imagery, we have to be aware that two main conditions need to be preserved. Those relate to the parallelism of the imaging planes, and to an accounting for projective discrepancies between central-perspective and affine projection. The following subsections briefly address these issues.

3.1 Satellite trajectory and object coordinate system

The satellite's trajectory is based on Keplar's motion and is non-linear in a Cartesian frame. This indicates that the direction of the pointing angle of the sensor with respect to the directions of the Z-axis (or the height direction) of the object coordinate system is time variant. In other words, the imaging planes are not parallel to each other. Furthermore, in a Cartesian system the distance to the curved ground surface is not constant, which in turn implies that the scale factor involved in Equation 1 cannot be constant for the entire scene. Therefore, the affine model could experience accuracy degradation when employed in a Cartesian frame. The use of additional parameters or the subdividing of an image strip into several sections, with the discrepancy level below a given tolerance, can offer solutions to this problem (Hattori et al., 2003).

As it happens, the parallelism of image planes is better preserved in a map projection system (map grid coordinates and ellipsoidal height). This is because the conformal map projection can be viewed as a cylindrical projection. A conformal map grid system such as UTM is a flat plane which is obtained by unfolding a cylinder wrapped around the ellipsoid at the central meridian. Considering that an orbital ellipse for the imaging satellite has a focus at the centre of mass of the earth, and has a small eccentricity, the view direction of the sensor with respect to the normal to the Earth's ellipsoid does not change drastically. Hence, the constructed image planes retain near-parallelism in a map projection reference system.

There are other important concerns relating to the orbital trajectory. Among these are the effects of perturbed motion of the sensor during image acquisition. For instance, if the roll angle ω changes continuously, a skew distortion will appear on the image. This type of skew distortion is also caused by earth rotation. Although the combined effects of all possible orbital perturbations can be complex, the affine model has shown itself capable of absorbing the perturbations of a fixed (non-agile) sensor to a considerable extent. On the other hand, if the sensor is steerable (agile), care has to be taken with the application of the affine model, which basically has the form of a simple linear transformation. This issue will be further discussed in Section 3.3.

It also follows that utilization of a geographic coordinate system with the affine model is not desirable because of its non-linear nature. From the standpoint that the affine model can be regarded as a special case of the third-order rational function model, it may well require higher-order terms when employed in a geographic coordinate system. For a nominal scene of HRSI, the author's experience suggests that accuracy degradation will be anticipated in both a geographic reference system (latitude, longitude, height) or in a local tangential system (X,Y,Z) (Hanley et al., 2002).

3.2 Projective discrepancies

For affine theory to be rigorously applicable to the orientation of line scanner imagery, it is mandatory that the projection discrepancy between a central-perspective and an affine projection be compensated (Okamoto et al., 1992). The relationship between a central perspective and an affine coordinate is illustrated for the scan line direction in Figure 1, where the projective relationship between a ground point and a line scanner image is shown at unit scale. The ground point P is projected onto the image point p by a central perspective projection and the image point p_a by an affine projection.

The central perspective image coordinate y can be converted to the affine image coordinate y_a by the following (Okamoto et al., 1992; Hattori et al., 2000; Fraser & Yamakawa, 2004):

$$y_a{}^0 = \frac{1}{1 - \frac{y \cdot \tan\omega}{f}} \cdot y \qquad (2)$$

$$y_a = \left(1 - \frac{\Delta Z_{scaled}}{\cos\omega}\right) y_a{}^0 \qquad (3)$$

where y = central-perspective coordinate
y_a, y_a = affine coordinate without/with height correction
f = focal length
ω = roll angle of the sensor
ΔZ = height from the average height of terrain

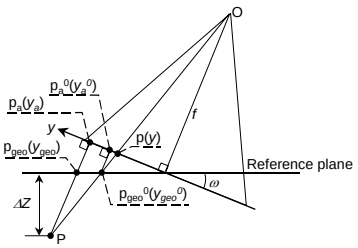

Figure 1. Conversion from central-perspective to affine imagery

Equations 2 and 3 are required for the central-perspective to affine image conversion. It can be seen that the correction becomes more important when either the roll angle or field of view of the sensor are large (Equation 2) or the terrain is mountainous (Equation 3). In other words, for a high-resolution sensor with a near-nadir view direction over low relief terrain, the perspective-to-affine image correction becomes negligible and conversion is not warranted. Of importance in an evaluation of the impact of the conversion is the invariance of the coefficients in Equations 2 and 3 (Fraser & Yamakawa, 2004).

If the image is georectified to a reference plane, which is the case for IKONOS *Geo* and QuickBird *Standard* imagery, the georectified point $p_{geo}{}^0$ is observed instead of p. Note that there is a linear relationship between the y-coordinate (sample coordinate) of $p_{geo}{}^0$ and $p_a{}^0$ ($y_a = y_{geo}\cos\omega$). This means that the correction of Equation 2 is implicit in the generation of georectified imagery. An image conversion for georectified imagery is therefore not required for moderately flat terrain. This is consistent with findings of practical applications employing IKONOS imagery (Fraser et al., 2002). However, for mountainous terrain, the image conversion may well have an impact upon geopositioning accuracy, as will be shown later.

A 'rigorous' theory for satellite sensor orientation based on affine projection has also been proposed by Zhang & Zhang (2002). As it happens, the conversion coefficient in their model is of the same form as that in Equations 2 and 3 (Fraser & Yamakawa, 2004).

3.3 Sensor dynamics

Agile HRSI satellites can dynamically rotate and swing so that the sensor is tilted to 20-40 degrees off nadir. This has advantages of shortening the revisit period and offering flexible imaging configurations, including along-track stereo recording. The ability to view obliquely is quite common for earth observation satellites and is, needless to say, required for across-track stereo coverage. A concern arising here in the context of the affine model is the possible introduction of non-linear perturbations as a result of dynamically re-orienting the satellite during image recording. IKONOS offers two imaging modes: 'Forward mode' and 'Reverse mode'. In the Forward mode, the sensor pointing direction is moving backwards, opposite to the satellite motion and changing at around one degree per second. In 'Reverse mode' the sensor is close to steady, maintaining a near constant view direction.

In terms of geometrical characteristics, dynamic variation in pitch angle requires special attention because it could cause non-uniform resampling. Although imagery products are georectified by utilising a very rigorous sensor geometry model, high frequency accelerations or perturbations of the sensor might not always be perfectly recovered and completely corrected for in the imagery. This concern is more pronounced with QuickBird, simply because of its continuous re-orientation during image capture.

The standard formulation of the affine model treats the orientation parameters as time-invariant. However, as an approach to accounting for the presence of non-linear image perturbations, time-variant coefficients can be considered:

$$\begin{aligned} x &= A_1(t)X + A_2(t)Y + A_3(t)Z + A_4(t) \\ y &= A_5(t)X + A_6(t)Y + A_7(t)Z + A_8(t) \end{aligned} \qquad (4)$$

where $A_i(t) = a_0{}^i + a_1{}^i t = a_0{}^i + b_1{}^i x \qquad (5)$

For geometrical interpretation, Equation 4 can be rearranged to:

$$\begin{aligned} &(a_0{}^1X + a_0{}^2Y + a_0{}^3Z + a_0{}^4 - x) + x(b_1{}^1X + b_1{}^2Y + b_1{}^3Z + b_1{}^4) = 0 \\ &(a_0{}^5X + a_0{}^6Y + a_0{}^7Z + a_0{}^8 - y) + x(b_1{}^5X + b_1{}^6Y + b_1{}^7Z + b_1{}^8) = 0 \end{aligned} \qquad (6)$$

where $\Pi_1 = a_0{}^1X + a_0{}^2Y + a_0{}^3Z + a_0{}^4 = 0$ relates to the image plane in line direction at $x = 0$
$\Pi_2 = a_0{}^5X + a_0{}^6Y + a_0{}^7Z + a_0{}^8 - y = 0$ relates to the image plane(s) in sample direction at $x = 0$

As illustrated in Figure 2, in the line (across-track) direction the imaging plane $\Pi_1'(a_0{}^1X + a_0{}^2Y + a_0{}^3Z + a_0{}^4 - x = 0)$, which is parallel to Π_1, rotates around an axis defined as an intersection of planes Π_1' and $\Pi_3\,(b_1{}^1X + b_1{}^2Y + b_1{}^3Z + b_1{}^4 = 0)$, as time goes on. Similarly, in the sample direction the imaging plane Π_2 rotates around an axis defined as an intersection of planes Π_2 and $\Pi_4\,(b_1{}^5X + b_1{}^6Y + b_1{}^7Z + b_1{}^8 = 0)$.

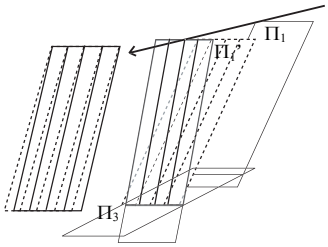

Figure 2. Geometrical interpretation of time-variant affine parameters.

The affine model with time-variant parameters requires eight GCPs instead of the usual four. The significant rise in the number of unknown parameters is not too desirable in terms of the numerical stability of the computation. Equation 4, therefore,

should be viewed as a generalised form of the extended affine model. In some circumstances, constraints may need to be imposed on certain parameters to enhance model stability. For instance, if the object space system is locally shifted to the scene centre, the constant terms of the planes Π_3 and Π_4 could become close to zero meaning that the parameters A_4 and A_8 may then need to be constrained as time-invariant.

Equation 4 can be supplemented with additional parameters to describe quadratic or possibly higher-order error effects. These can be cast as functions of either image or object space coordinates. The choice of additional parameters depends upon the type of sensor. However, the first priority for the affine model would be four quadratic terms. In this case, the extended formulation is expressed as follows:

$$l = A_1(t)X + A_2(t)Y + A_3(t)Z + A_4(t) + B_1 l^2 + B_2 s^2 \quad (7)$$
$$s = A_5(t)X + A_6(t)Y + A_7(t)Z + A_8(t) + B_3 l^2 + B_4 s^2$$

where A_i, B_i = time-variant/invariant parameters
l, s = line, sample coordinates
X,Y,Z = object space coordinates

Geometrically, the adoption of the additional parameters allows the image planes Π_1' and Π_2 to be curved. Further investigation will provide more insight into the connection between the affine and higher-order rational polynomial models.

4. EXPERIMENTS

4.1 Overview

To verify the applicability of the affine model to HRSI, three sets of testfield HRSI data have been investigated. The aims of the experiments were, first, to ascertain the degree of accuracy degradation, if any, of the affine model when employed in mountainous terrain; and, second, to evaluate the extended form of the affine model (Equation 7) for QuickBird *Basic* imagery. Table 1 summarises the testfield data involved in the experiments. Further details of the testfields can be found in Fraser et al. (2002), Noguchi et al. (2004) and Fraser & Yamakawa (2004).

	Hobart	Melbourne	Yokosuka
Area	120 km^2 (11 x 11)	300 km^2 (17.5x17.5)	300 km^2 (17.5x17.5)
Elevation	1280 m	50 m	170 m
No. of GCP/CPs	110 points by GPS	81 points by GPS	61 points by GPS
Types of feature point	Mainly road roundabouts	Mainly road roundabouts	Mostly corner features
Image coverage	IKONOS Geo stereo pair B/H = 0.8	QB basic stereo pair B/H = 1.0	QB basic stereo pair B/H = 1.0
Image Meas.	Digital mono comparator (estimated accuracy of 0.2 pixel)		

Table 1. Summary of the Hobart, Melbourne and Yokosuka testfields.

4.2 Results with IKONOS

The results of affine bundle adjustments of the IKONOS *Geo* stereo pair imagery covering Hobart (captured in Reverse mode) are listed in Table 2. Because of the mountainous nature of the terrain, the standard affine formulation coupled with the iterative height correction approach (Subsection 3.2) was employed. To assess the effect of the projection discrepancies due to the influence of terrain, the standard formulation without the height correction was also applied (numbers in brackets in Table 2). It should be noted that several GCP configurations were tested for each GCP set (same number of control points), except for the case of all GCPs. The RMS discrepancies and standard errors shown in each row of Tables 2 and 4 are representative values for each GCP set and they are calculated from independent checkpoints only. The term "RMS_{xy}" in Tables 2 and 4 denotes the RMS value of image coordinate residuals from the bundle adjustment.

GCP (CP)	RMS_{xy} pixels	Std. errors at checkpoints (m)	RMS discrepancies at checkpoints (m)
		σ_E / σ_N / σ_H	S_E / S_N / S_H
All (-)[*1)]	0.13	- / - / -	0.54 (0.76) / 0.34 / 0.56
9 (101)	0.13	0.49 / 0.46 / 0.85	0.62 (0.83) / 0.43 / 0.73
6 (104)	0.13	0.56 / 0.50 / 0.86	0.62 (0.84) / 0.41 / 0.72
4 (106)	0.13	0.77 / 0.75 / 1.19	0.62 (0.90) / 0.42 / 0.77
9 GCPs, none on Mt Wellington (101 checkpoints)			
9 (101)	0.13	0.70 / 0.65 / 1.06	0.70 (0.83) / 0.46 / 1.10

*1) *All GCPs loosely weighted (σ = 3 m)*

Table 2. Results of affine bundle adjustments for IKONOS *Geo* stereo image pair covering the Hobart testfield.

Overall, sub-pixel accuracy was achieved for all GCP sets, except for the case of 9 GCPs where none of the control points were selected from the Mt. Wellington area. The height correction produced an accuracy improvement in RMS geopositioning of about 0.2m in the Easting direction. This is because the image conversion for the height correction directly affects the sample coordinates, which correspond to the Easting direction in this case. To illustrate the effect of the height correction, the planimetric RMS discrepancy vectors from the all-GCPs bundle adjustment (the 1st row of Table 2) are plotted in Figure 3 for the cases of with and without height correction.

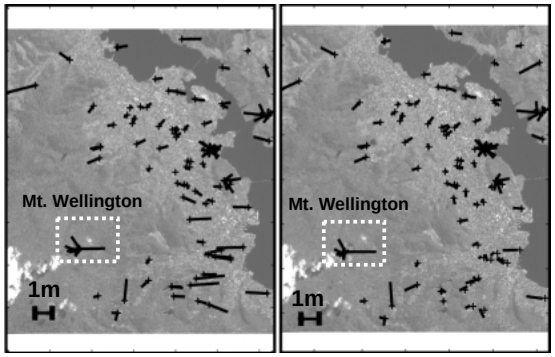

a) Without height correction b) With height correction

Figure 3. Plots of planimetric discrepancy vectors for the all-GCP bundle adjustment, Hobart IKONOS image.

Figure 3a illustrates that a systematic trend is evident in the residual vectors in the Easting (across-track) direction, especially in the surroundings of 1300m high Mt. Wellington, whereas this error signal is substantially reduced when the height correction is undertaken (Figure 3b). This supports the view that projection discrepancies caused by the height undulation are largely removed by the image conversion. However, even with the height-correction the RMS values are still marginally higher in Easting than in Northing. One of the reasons for this is attributed to errors in the image conversion arising from uncertainty in the value of the roll angle of the sensor utilised for the computation of the height-corrected y-coordinate. However, the accuracy achieved is still considered to be impressive from a practical point of view. In fact, it is noteworthy that sub-pixel accuracy was attained with the standard formulation, Equation 1 (ie. without the height correction).

4.3 QuickBird results

As mentioned in Section 3.3, it is expected that QuickBird imagery will be more prone to adverse effects from dynamically changing sensor orientation. To first verify the presence of an error signal from the sensor dynamics, and to quantify its magnitude in the imagery, spatial resections were computed for three formulations of the affine model: 1) the standard 8-parameter affine, 2) the extended affine with time-variant parameters, and 3) the extended model with additional parameters. The resulting RMS values of image coordinate residuals are listed in Table 3.

It is apparent from the results in Table 3 that non-linear error influences are present and that these cannot be fully compensated via a standard affine formulation, Equation 1. In fact, the implementation with time-variant affine parameters and additional parameters is required to yield satisfactory results. It can also be seen that the magnitude of the non-linearity induced image coordinate errors is case-dependent, ranging here from roughly 5 to 16 pixels.

Formulation	RMS of image residuals (pixels)	
	Left	Right
QuickBird Melbourne		
Standard	15.26	5.38
Time-variant parameters	7.99	2.48
Time-variant parameters plus AP	0.37	0.22
QuickBird Yokosuka		
Standard	10.40	15.95
Time-variant parameters plus AP	0.46	0.60

Table 3. Resection residuals from the affine model.

In light of the results in Table 3, the extended formulation of the affine model with additional parameters was adopted for the bundle adjustments of the QuickBird *Basic* stereo pairs. The results of these adjustments are listed in Table 4. Figure 4 shows plots of the residual image coordinate error vectors from the bundle adjustment for the all-GCPs case (the 1st row of results in each testfield). The systematic trends exhibited in the plots of residuals, which show approximate alignment with the satellite track direction, suggest the existence of higher-order sensor perturbations, which cannot be modelled by the extended affine model, Equation 7. Similar, though much smaller systematic error trends have also been seen in RPC bundle adjustments of QuickBird stereo imagery (Fraser & Hanley, 2004).

Number of GCPs (CP)	RMS_{xy} (pixels)	Std. errors at checkpoints (m)	RMS discrepancies at checkpoints (m)
		σ_E / σ_N / σ_H	S_E / S_N / S_H
QuickBird Melbourne stereo			
All (-)*1)	0.13	- / - / -	0.22 / 0.24 / 0.37
15 (66)	0.16	0.16 / 0.15 / 0.24	0.26 / 0.29 / 0.42
12 (69)	0.16	0.17 / 0.15 / 0.26	0.25 / 0.32 / 0.41
10 (71)	0.16	0.18 / 0.15 / 0.26	0.32 / 0.36 / 0.43
QuickBird Yokosuka stereo			
All (-)*1)	0.17	- / - / -	0.37 / 0.40 / 0.48
15 (46)	0.20	0.17 / 0.21 / 0.36	0.50 / 0.48 / 0.60
12 (49)	0.19	0.19 / 0.23 / 0.39	0.49 / 0.47 / 0.56
10 (51)	0.19	0.21 / 0.26 / 0.43	0.49 / 0.48 / 0.54

*1). *All GCPs loosely weighted (σ = 2 m)*

Table 4. Results of affine bundle adjustments of QuickBird *Basic* imagery of Melbourne and Yokosuka testfields.

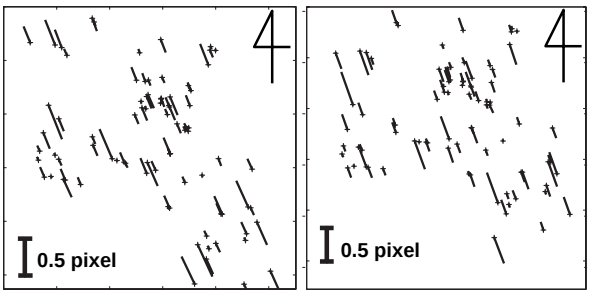

Left stereo Right stereo

a) Melbourne

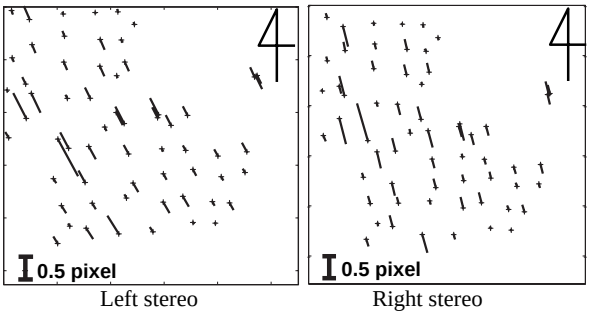

Left stereo Right stereo

b) Yokosuka

Figure 4. Plots of image coordinate residuals from affine bundle adjustment for QuickBird (case of all GCPs).

5. CONCLUSION

This paper has discussed three formulations of the affine model for HRSI sensor orientation, and summarized results obtained with this empirical approach for geopositioning. In the context

of ongoing developments involving the affine model, two principal issues have been dealt with. The first concerns the impact of a height correction for image coordinates, which arises from the discrepancy between an affine and central-perspective projection. The second relates to the potentially adverse effects on the standard affine model of dynamic re-orientation of the satellite during image recording. These effects can, however, be modelled to reasonable accuracy via time-variant affine parameters, along with four quadratic additional parameters and the recommendation that the object space coordinates be in a projection system such as UTM.

Finally, experimental application of affine bundle adjustments to one IKONOS and two QuickBird stereo image pairs have illustrated both the advantages and potential shortcomings of the affine model, in both its standard and extended forms. The results from the IKONOS Hobart testfield have shown that the affine model does not cause significant accuracy degradation, even over terrain with an elevation range of 1300m. Moreover, while the perspective-to-affine image correction procedure leads to accuracy improvements, these amounted in Hobart to only about 0.2 pixels in the across-track direction.

On the other hand, it was found for QuickBird *Basic* imagery that the extended formulation of the affine model with four additional parameters, Equation 7, was needed to produce sub-pixel accuracy. This also required 10 to 15 GCPs. The accuracy achieved from the experiments overall is essentially equivalent to that obtained with the more rigorous RPC model (eg Fraser & Hanley, 2004; Noguchi et al., 2004). These encouraging results lend weight to the view that the affine model is a practical sensor orientation model that should, however, be used with some caution for QuickBird *Basic* and IKONOS Forward scanned imagery.

6. ACKNOWLEDGEMENTS

The authors wish to thank Digital Globe, Space Imaging and the Geographical Survey Institute of Japan, respectively, for providing the HRSI stereo pairs of Hobart, Melbourne and Yokosuka.

7. REFERENCES

Fraser, C.S., Hanley, H.B. and T. Yamakawa, 2002. 3D positioning accuracy of IKONOS imagery. *Photogrammetric Record*, 17(99): 465-479.

Fraser, C.S. and H.B. Hanley, 2004. Bias compensated RPCs for sensor orientation of high-resolution satellite imagery. *Proc. ASPRS Annual Conference*, Denver, 9 pages (on CD-ROM).

Fraser, C.S. and T. Yamakawa, 2004. Insights into the affine model for satellite sensor orientation. *ISPRS Journal of Photogrammetry & Remote Sensing* (in Press)

Grodecki, J. and G. Dial, 2003. Block adjustment of high-resolution satellite images described by rational functions. *Photogramm. Engineering and Remote Sensing*, 69(1): 59-68.

Hanley, H.B., Yamakawa, T. and Fraser, C.S. 2002. Sensor Orientation for High-Resolution Satellite Imagery. *Int. Archives of Photogramm. and Remote Sensing*, 34(1): 69-75.

Hattori, S., Ono, T., Fraser, C.S. and H. Hasegawa, 2000. Orientation of high-resolution satellite images based on affine projection. *Int. Archives of Photogramm. and Remote Sensing*, 33(3): 359-366.

Hattori, S., Yamakawa, T., Ono, T. and H. Hasegawa, 2003. Orientation of satellite line scanner images based on affine projection. *Technical paper, Japan Society of Civil Engineers*, 730(59): 1-13.

Noguchi, M., Fraser, C.S., Nakamura, T., Shimono, T. and S. Oki, 2004. Accuracy assessment of Quickbird stereo imagery. *Photogrammetric Record*, 17(98): 317-329.

Okamoto, A., Akamatsu, S. and H. Hasegawa, 1992. Orientation theory for satellite CCD line-scanner imageries of mountainous terrain. *Int. Archives of Photogramm. and Remote Sensing*, 29(2): 205-209.

Okamoto, A., Fraser, C.S., Hattori, S., Hasegawa, H. and T. Ono, 1998. An alternative approach to the triangulation of SPOT imagery. *Int. Archives of Photogramm. and Remote Sensing*, 32(4): 457-462.

Okamoto, A., Fraser, C.S., Hattori, S., Hasegawa, H. and T. Ono, 1999. Geometric characteristics of alternative triangulation models for satellite imagery. *Proc. ASPRS Annual Conference*, Portland, 12 pages (on CD-ROM).

Ono, T. and S. Hattori, 2003. Fundamental principle of image orientation using orthogonal projection model. *Int. Archives of Photogramm. and Remote Sensing*, 34(3), 6 pages (on CD-ROM).

Zhang, J. and X. Zhang, 2002. Strict geometric model based on affine transformation for remote sensing image with high resolution. *Int. Archives of Photogramm. and Remote Sensing*, 34(3): 309-312.